Applied Physics Letters

Temperature-dependent and polarization-tuned resistive switching in Au/$BiFeO_3$/$SrRuO_3$ junctions

Cite as: Appl. Phys. Lett. **104**, 143503 (2014); https://doi.org/10.1063/1.4870813
Submitted: 03 December 2013 . Accepted: 28 March 2014 . Published Online: 08 April 2014

Y. B. Lin, Z. B. Yan, X. B. Lu, Z. X. Lu, M. Zeng, Y. Chen, X. S. Gao, J. G. Wan, J. Y. Dai, and J.-M. Liu

Temperature-dependent and polarization-tuned resistive switching in $Au/BiFeO_3/SrRuO_3$ junctions

Y. B. Lin,[1] Z. B. Yan,[2,a)] X. B. Lu,[1] Z. X. Lu,[1] M. Zeng,[1] Y. Chen,[3] X. S. Gao,[1,a)] J. G. Wan,[2] J. Y. Dai,[3] and J.-M. Liu[2]
[1]*Institute for Advanced Materials and Laboratory of Quantum Engineering and Quantum Materials, South China Normal University, Guangzhou 510006, China*
[2]*Laboratory of Solid State Microstructures, Nanjing University, Nanjing 210093, China*
[3]*Department of Applied Physics, Hong Kong Polytechnic University, Hong Kong, China*

(Received 3 December 2013; accepted 28 March 2014; published online 8 April 2014)

The relationship between the bipolar resistive switching and the polarization reversal is investigated at various temperatures in the $Au/BiFeO_3/SrRuO_3$ structure. It is found that the polarization-induced barrier variation in the $Au/BiFeO_3$ and $BiFeO_3/SrRuO_3$ junctions decreases with decreasing temperature. This explains why the resistance-switching ratio decreases with decreasing temperature below 323 K and gives evidence that the polarization modulates the resistance state of the $Au/BiFeO_3/SrRuO_3$ structure. Besides, the oxygen vacancies migration and/or the carrier trapping/detrapping mechanisms are also suggested to play a very important role in the resistive switching behavior in this structure as the temperature goes above 323 K. © *2014 AIP Publishing LLC*. [http://dx.doi.org/10.1063/1.4870813]

As one of the next-generation nonvolatile memories, resistance-switching random access memory (RRAM) has attracted much attention due to its simple structure, good performance, and potential process compatibility with the conventional semiconductor technologies.[1–6] Besides the binary transition metal oxides,[7] the resistive switching phenomena are also observed in perovskite oxides, such as $Pr_{0.7}Ca_{0.3}MnO_3$,[8] $BaTi_{1-x}Co_xO_3$,[9] $BiFeO_3$(BFO),[10] and so on. BFO has been widely investigated over the last decade because of its excellent multiferroic properties at room temperature.[11] Nevertheless, the actual ferroelectric memory applications of BFO film are greatly limited by its high coercive electric field and high leakage current.[12] Recently, the electric field induced resistive switching behaviors are observed in the BFO thin films, which gives a new idea to utilize its ferroelectricity and high leakage current.[13–23] For the other transitional ferroelectric materials such as $BaTiO_3$, the large bandgap of them gives very tiny leakage and/or tunneling current and hence ultrathin ferroelectric film is needed for the *dc* resistance reading. In the metal/BFO/metal sandwiched structures, however, the high leakage current of BFO means that the ultrathin BFO film is not a pre-requisite for the convenient *dc* resistance reading.

Several mechanisms are suggested to explain the resistive switching behaviors in metal/BFO/metal structures, involving the formation/rupture of conductive filaments,[13–15] the carrier- and/or defect-induced modulation of the depletion layer thickness,[16] the charge trapping/detrapping,[17] and the polarization direction dependent tunneling effect.[18–23] In these resistive switching mechanisms, the ferroelectric polarization reversal possesses a fundamental merit over defect-mediated mechanisms (ionic or electronic) for reliable performance required in commercial production, since ferroelectric polarization reversal is based on the intrinsic ferroelectric domains without invoking of the charged defects immigration.[21,22] It is suggested that the electric field induced polarization reversal changes the charge distributions at metal/ferroelectric interface and modulates the junction barrier profile, which leads to the nonvolatile change of leakage and/or tunneling currents and, as a result, presents the resistive switching behavior.[18–23] However, the detail understandings on the relation between the polarization reversal and the resistive switching is still lacking, and the more convincing experimental evidence is needed.

In this work, the $Au/BFO/SrRuO_3$(SRO) sandwiched structures were fabricated, and the relation between the ferroelectric polarization and the resistive switching were investigated under various temperatures. Our experimental results indicate that the polarization-induced barrier variation in the Au/BFO and BFO/SRO junctions decreases with decreasing temperature, which explains why the resistance switching ratio also shows a similar trend below 323 K and provides evidence that the polarization modulates the resistance state of the $Au/BiFeO_3/SrRuO_3$ heterostructure.

The polycrystalline BFO thin films were grown on SRO/Pt substrates by pulsed laser deposition. The crystalline phase was checked by X-ray diffraction, and no impurity phases have been observed within the X-ray diffraction detection limit. Circular gold (Au) top electrodes with a diameter of 100 μm were fabricated by radio frequency sputtering at room temperature using a metal shadow mask. The current-voltage (*I-V*) characteristics were measured by a Keithley 6430 sub-femtoampere source meter. The voltage dependent ferroelectric polarization (*P-V*) hysteresis loops were measured by a Radiant ferroelectric tester Premier II with an 50 kHz *ac* driving voltage. The temperature dependent *I-V* and *P-V* measurements were carried out in a Jannis temperature variable probe station.

Figure 1(a) shows the typical *I-V* loop behavior of the Au/BFO/SRO heterostructure at room temperature, with the measuring configuration shown in the inset. By sweeping

a)Authors to whom correspondence should be addressed. Electronic addresses: zbyan37@gmail.com and xingsengao@scnu.edu.cn

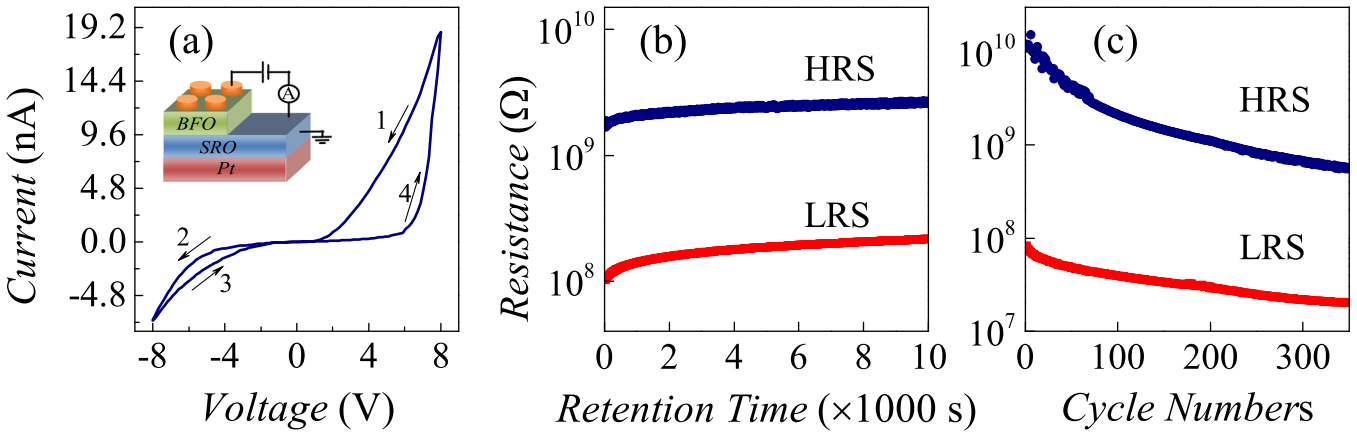

FIG. 1. (a) Typical *I-V* curve of the Au/$BiFeO_3$/SRO heterostructure at room temperature, with the sweeping sequence of 10V → −10V → 10 V. Inset illustrates the measurement configuration. (b) and (c) The endurance and retention characteristics of the Au/$BiFeO_3$/SRO heterostructure at room temperature, respectively, with the operating voltage of ±10 V and readout at 2.5 V.

the voltage from 8 V to −8 V, a rectifying behavior is observed. Then, as the voltage was swept back to 8 V (at which the polarization switching happens), another different rectifying *I-V* behavior is observed and then an anticlockwise *I-V* loop forms. This *I-V* loop indicates the bipolar resistance switching without a forming process, in which the positive voltage switches the device to a low resistance state (LRS) while the negative voltage switches it to a high resistance state (HRS). Besides, this *I-V* loop does not intersect at $V = 0$, which is very different from the conventional filament-type bipolar resistive switching behavior.[13,16] It is noted that the definitions of LRS and HRS are based on a positive reading voltage.

To assure this bipolar resistive switching behavior, we apply a 1.0 ms-width voltage pulse of +10 V (or −10 V) to the heterostructure and then measure the time dependent resistance of the LRS (or the HRS) with a reading voltage of 2.5 V, respectively. The resistances of the HRS and LRS are denoted by R_H and R_L, respectively. Figure 1(b) shows the retention of the HRS and the LRS over 10^4 s, in which the R_H/R_L ratio remains at about 30. Besides, the switching endurance characteristic is also shown in Figure 1(c), in which the switching is operated by the 1 ms-width ±10 V voltage pulses while the resistance is readout at 2.5 V. The switching between the LRS and the HRS is repeatable, and the R_H/R_L ratio has a weak decrease with the switching cycles but remains at about 30 even after 200 consecutive switching cycles. Hence, the device displays a reliable bipolar resistive switching behavior during the application of polar-reversed voltages.

The BFO films are assumed to be n-type semiconductors due to the possible existing oxygen vacancies which act as electron donors.[24] The electron affinity and the Fermi level of BFO are ∼3.3 eV and ∼4.7 eV, respectively, and the work functions of SRO and Au are ∼5.2 eV and ∼5.1 eV, respectively.[25,26] The differences of the electron affinity and/or the work function of BFO, SRO, and Au lead to the formation of the Schottky barrier at the Au/BFO and the BFO/SRO interfaces, as shown in Figures 2(a) and 2(b).[23] The different barrier heights of these two interfaces would lead to the appearance of the diode behavior in the Au/BFO/SRO heterostructure. By applying a positive (or negative) voltage to the Au electrode while the SRO electrode is grounded, a higher (or lower) junction barrier of the Au/BFO interface than that of the BFO/SRO interface gives a forward (or backward) diode behavior. Figure 2(c) shows the *I-V* behaviors of both the LRS and the HRS between −2 V and 2 V which are small enough to retain the device resistance state. The LRS displays a forward diode behavior while the HRS shows a backward diode behavior, consistent with earlier reports.[18,23] These reversed rectification behaviors imply that the relative barrier heights between the Au/BFO and the BFO/SRO junctions are varied after the switching between the LRS and the HRS.

It was previously suggested that the ferroelectric polarization reversal of the BFO layer modulates the barrier profiles of the SRO/BFO and Au/BFO junctions.[23,27,28] If the ferroelectric polarization points to the SRO [Figure 2(a)], the positive polarization charges induce the accumulation of electrons near the BFO/SRO interface due to the depolarization field. As a result, the depletion width in the BFO side is narrowed and the BFO/SRO junction barrier height and width are reduced. In the meantime, the negative polarization

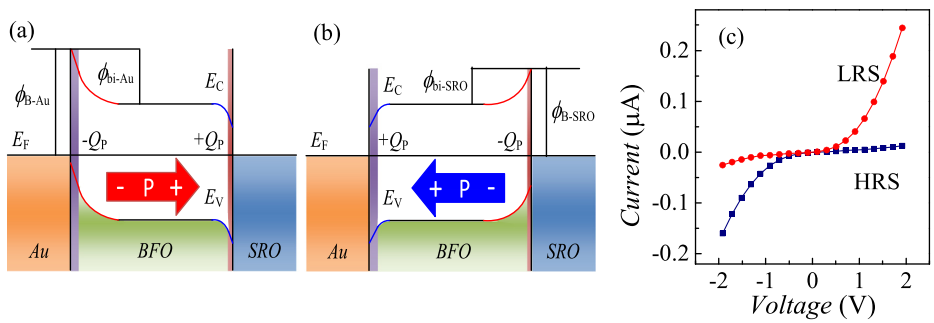

FIG. 2. (a) and (b) Schematic diagrams of energy band structure of the Au/BFO/SRO heterostructure, with the situations of the downward and the upward polarization states, respectively. (c) Rectifying *I-V* behaviors of the LRS and the HRS.

charges at other BFO side spread the space depletion region and raise the barrier height/width of the Au/BFO junction. Therefore, the asymmetrical junction barriers in the Au/BFO and BFO/SRO interfaces give to a positive diode behavior. With a positive reading bias, the electrons can easily flow through the BFO/SRO and Au/BFO junctions, forming the LRS.

Similarly, as the polarization is reversed, i.e., pointing to the Au electrode [Figure 2(b)], the negative polarization charges deplete the electrons and spread the space depletion region near the BFO/SRO interface, leading to the increase of the junction barrier height and width. While at the Au/BFO interface, however, the positive polarization charges accumulate the electrons at the BFO side and consequently reduce the barrier of Au/BFO junction. Thus, the relative barrier height of the Au/BFO and BFO/SRO junction is varied, and a reversed diode behavior is demonstrated. In this situation, a positive reading bias results in a low current, i.e., the HRS.

The application of an external voltage (larger than the coercive voltage) not only changes the ferroelectric polarization of BFO film but also leads to the resistive switching in the Au/BFO/SRO heterostructure. To explore the relation between the resistive switching and the BFO ferroelectric polarization reversal, the *I-V* and *P-V* loops with various voltage sweeping ranges were measured on a same device cell at room temperature. Figure 3(a) shows the *I-V* loops with the maximum voltage $V_{max} = 3$ V, 5 V, 8 V, 10 V, and 12 V, respectively. It is seen that the remarkable *I-V* hysteresis loop appears as $V_{max} \geq 8$ V and disappear as $V_{max} \leq 5$ V. Similarly, the *P-V* hysteresis loop is only observed as the V_{max} is larger than the coercive field (i.e., $V_{max} \geq 8$ V), as shown in Figure 3(b). For the convenient comparison, the area of the *I-V* and *P-V* hysteresis loops is calculated. Figure 3(c) shows that the *I-V* and *P-V* loop areas remain at zero as $V_{max} \leq 5$ V and then rapidly increase as $V_{max} \geq 8$ V, suggesting a strong relation between the resistive switching and the polarization switching.

Under the modulation of ferroelectric polarization, the build-in potential of the metal/n-type semiconductor junction is given by $\phi'_{bi} = \phi_{bi} + \Delta\phi_{bi}^{P} = \phi_{bi} \pm P\delta/\varepsilon_0\varepsilon_s$,[29,30] where ϕ_{bi} is the built-in potential in the absence of the polarization charges, $\Delta\phi_{bi}^{P}$ is the variation of the build-in potential induced by the polarization, ε_0 is the permittivity of free space, ε_s is the low-frequency (static) dielectric constant, P is the ferroelectric polarization, and δ is the width between the polarization surface charge and the physical interface with electrode. For the metal/n-type ferroelectric semiconductor junctions like the Au/BFO and BFO/SRO junctions, the upper sign is for the negative polarization charges and the lower sign is for the positive polarization charges. Therefore, besides the polarization direction, the variation of polarization in magnitude changes the build-in potential and the junction's resistance as well. This well explains why a larger polarization brings out a larger resistance variation as shown in Figures 3(a) and 3(b).

To evidence the relation of the junction resistive switching with the BFO ferroelectric polarization reversal, the *P-V* and *I-V* loops at various temperatures from 123 K to 373 K were measured at a same device cell. Figure 4(a) shows the

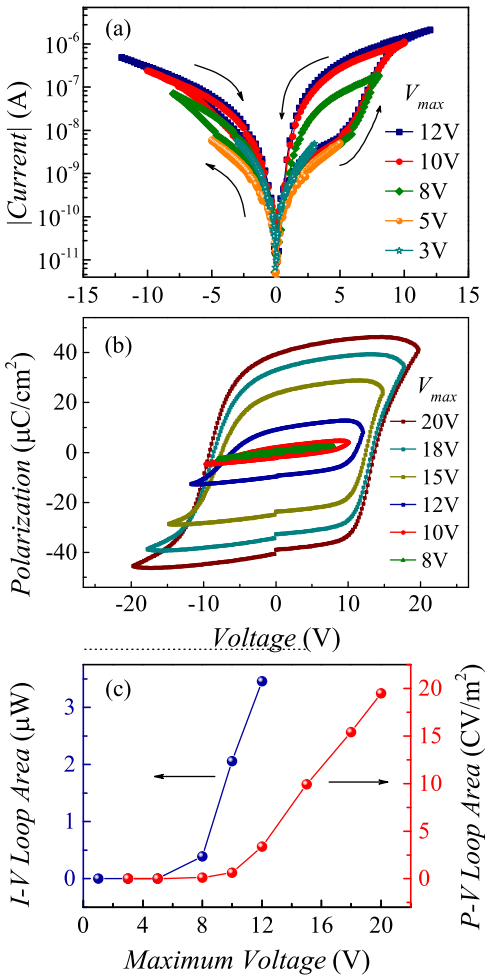

FIG. 3. (a) *I-V* loops at room temperature, with $V_{max} = 3$ V, 5 V, 8 V, 10 V, and 12 V, respectively. (b) *P-V* loops at room temperature, measured at 50 kHz with $V_{max} = 8$ V, 10 V, 12 V, 15 V, 18 V, and 20 V, respectively. (c) The V_{max} dependent areas of the *I-V* loop and the *P-V* loop.

P-V loops that were measured under a fixed *ac* voltage. The remnant polarization (P_r), extracted from the *P-V* data, decreases with decreasing temperature, as shown in Figure 4(b). Besides, the data of the temperature dependent low-frequency dielectric constants ε_s are shown in the inset of Figure 4(b), and the δ can be supposed to be temperature independent and estimated to be 1 nm.[20,31] With these data, the $\Delta\phi_{bi}^{P} = P_r\delta/\varepsilon_0\varepsilon_s$ is calculated, which increases with the temperature, as shown in Figure 4(b).

The *I-V* loops were measured in a sequence of 15V → −15V → 15 V with a sweep-rate of 0.8 V/s. By lineally fitting the *I-V* data between 2.0 V and 3.0 V at various temperatures, the temperature dependent resistances of the HRS and the LRS were obtained, as shown in Figure 4(c). The semiconductor/insulator behaviors of the HRS and the LRS agree with the above understanding that both the HRS and the LRS are limited by the interface barrier height. Furthermore, the R_H/R_L ratio increases with the temperature below the 323 K, which is consistent with the temperature dependency of $\Delta\phi_{bi}^{P}$ because the increase of $\Delta\phi_{bi}^{P}$ implies the enlargement of the difference between the HRS and the LRS (i.e., the raise of the R_H/R_L ratio). Therefore, the mechanism that the polarization reversal modulates the resistive switching behavior is evidenced.

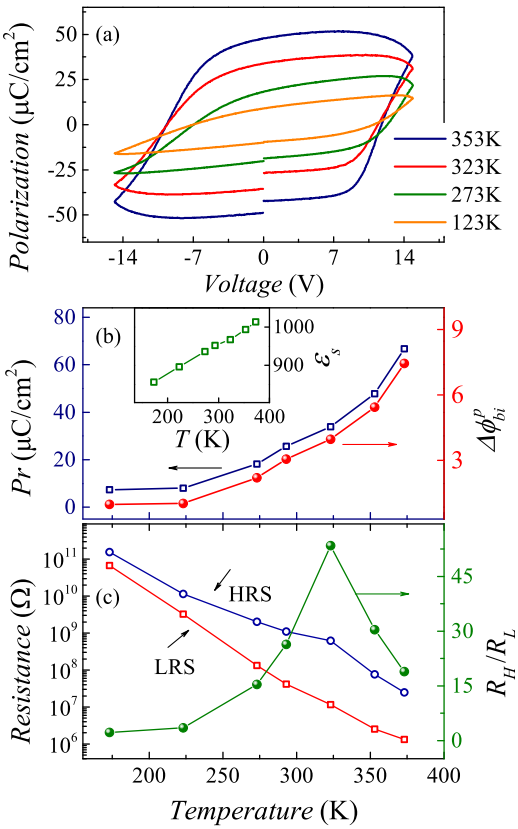

FIG. 4. (a) *P-V* loops under different temperatures. (b) Temperature dependent P_r, ε_s, and $\Delta\phi_{bi}{}^P$. The P_r data are extracted from (a) and the $\Delta\phi_{bi}{}^P$ is the calculated result. (c) Temperature dependent R_H, R_L, and R_H/R_L ratio. R_H and R_L data are calculated by linearly fitting the *I-V* data from 2 V to 3 V at various temperatures.

As the temperature is above 323 K, however, the R_H/R_L ratio decreases with increasing the temperature, which can be well explained by the migration of oxygen vacancies and/or the carrier trapping/detrapping near the metal/semiconductor interface.[6,9,32–34] For these resistive switching mechanisms, both the HRS and the LRS can be simply described by the Arrhenius thermal activation model,[35,36] i.e., $\ln(R_H) \propto \varepsilon_{aH}/T$ and $\ln(R_L) \propto \varepsilon_{aL}/T$, with $\varepsilon_{aH} > \varepsilon_{aL}$ for satisfying $R_H > R_L$, where ε_{aH} and ε_{aL} are the activation energies. So, $\ln(R_H/R_L) \propto (\varepsilon_{aH} - \varepsilon_{aL})/T = \Delta\varepsilon/T$. Thus, the R_H/R_L ratio increases with decreasing the temperature.

To further confirm that the resistive switching mechanisms in the Au/BFO/SRO heterostructure, we measured the voltage sweep-rate dependent *I-V* loops at different temperatures. Figure 5(a) shows the hysteretic *I-V* curves under different sweep-rates at 173 K. The clockwise *I-V* rotation is observed, and the current peaks appear at around the coercive voltages of $\sim\pm9$ V, which is in association with the polarization reversal. Besides, the peak current distinctly increases with the sweep-rate from 0.8 V/s to 5 V/s, further confirming the domination of the ferroelectric switching. Under a faster voltage sweep, a larger transient current would be expected due to the polarization switching in a shorter time. It notes that the ferroelectric switching (in nanosecond time scale) is much faster than our voltage sweeping (in second time scale).

With temperature increasing up to 273 K [Figure 5(b)], a higher sweep-rate still leads to a little larger current but the differences under different sweep-rates are reduced. This feature implies that the transient current from the fast ferroelectric switching is still dominating at this temperature. As the temperature is raised to 323 K [Figure 5(c)], the differences in current under the rates of 0.8 V/s, 3.3 V/s, and 5 V/s disappear during the sweep of $0 \rightarrow 10\,\text{V} \rightarrow -10\,\text{V}$. In the next sweep of $-10\,\text{V} \rightarrow 0$, however, the current under the rate of 0.8 V/s is dramatically enlarged at −9 V from −381 nA to the compliance value (−1000 nA), which is much larger than those under higher sweep rates of 3.3 V/s and 5 V/s, indicating that a slower sweeping begins to produce a larger current. As the temperature is further increased to 373 K [Figure 5(d)], slower sweepings surely bring out a larger current, which is contrary to the situation below 273 K. These results clearly indicate the existence of "slow" mechanisms that play more and more important roles in the resistive switching as the temperature increases from 173 K to 373 K.

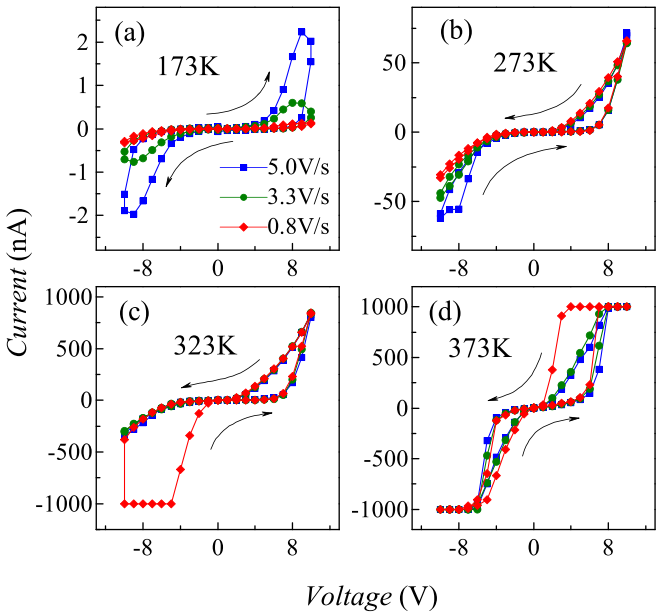

FIG. 5. *I-V* behaviors under the voltage sweep-rates of 0.8 V/s, 3.3 V/s, and 5 V/s, measured at the temperature of (a) 173 K, (b) 273 K, (c) 323 K, and (d) 373 K, respectively.

The uniform migration of oxygen vacancies and/or the carrier trapping/detrapping at the two interfaces of the metal/oxide/metal structure are the most possibly slow mechanisms that can lead to reversible diode effects without a forming process.[17,37] The migration time for the uniform oxygen vacancies decreases with the temperature, and can vary from $\sim10^9$ s (at ~300 K) to ~10 s (at ~500 K).[37] The relaxation time for the carrier trapping/detrapping is also above 100 s time.[6,17] Such long migration/relaxation times are consistent with the observations in Figure 5(d).

Besides, except for the ferroelectric switching mechanism, these two slow mechanisms can also change the nonvolatile resistance state and give rise to the anti-clockwise *I-V* rotation at high temperatures.[8,17,23] During the sweep of $0 \rightarrow V(V > 0) \rightarrow 0$, Figure 1 indicates that the HRS is changed to the LRS. Hence, the leakage current in the backward sweep ($V \rightarrow 0$) is larger than that in the forward sweep ($0 \rightarrow V$), which naturally causes the anti-clockwise *I-V*

rotation. Similarly, the nonvolatile resistance change would lead to the anti-clockwise *I-V* during the negative voltage sweeping, noting that the resistance read by negative voltage is also decreased after the negative voltage sweep.

In summary, we study the relation between the bipolar resistive switching and the polarization reversal in the Au/BFO/SRO heterostructures at different temperatures. By analyzing the temperature dependencies of the *Pr* and the R_H/R_L and the sweep-rate dependent *I-V* behaviors, we conclude that both the polarization modulation model and the migration of oxygen vacancies and/or carrier trapping/detrapping mechanisms are contributed to the bipolar resistance switching in the Au/BFO/SRO heterostructure. The resistance switching is dominated by the modulation of polarization in the temperature region below 323 K, in which the polarization charges change the barrier profile at the electrode/BFO junction interfaces. While above the 323 K, the migration of oxygen vacancies and/or the carrier trapping/detrapping mechanism play a very important role in the resistive switching behavior.

This work was supported by the National 973 Projects of China (Grant No. 2011CB922101), Natural Science Foundation of China (Grant Nos. 51031004, 51301084, and 51272078), Natural Science Foundation of Jiangsu and Guangdong, China (Grant Nos. BK20130576 and S2012010008124), and Program for Changjiang Scholars and Innovative Research Team in University, China (Grant No. IRT1243). J.Y.D. gratefully acknowledge financial support from the Hong Kong Research Grant Council (No. PolyU 514512).

[1]R. Waser and M. Aono, Nature Mater. **6**, 833 (2007).
[2]G. I. Meijer, Science **319**, 1625 (2008).
[3]R. Waser, R. Dittmann, G. Staikov, and K. Szot, Adv. Mater. **21**, 2632 (2009).
[4]D. S. Jeong, R. Thomas, R. S. Katiyar, J. F. Scott, H. Kohlstedt, A. Petraru, and C. S. Hwang, Rep. Prog. Phys. **75**, 076502 (2012).
[5]J. J. Yang, D. B. Strukov, and D. R. Stewart, Nat. Nanotechnol. **8**, 13 (2012).
[6]Z. B. Yan and J. M. Liu, Sci. Rep. **3**, 2482 (2013).
[7]D. B. Strukov, G. S. Snider, D. R. Stewart, and R. S. Williams, Nature **453**, 80 (2008).
[8]J. L. Gang, S. L. Li, Z. L. Liao, Y. Meng, X. J. Liang, and D. M. Chen, Chin. Phys. Lett. **27**, 027301 (2010).
[9]Z. Yan, Y. Guo, G. Zhang, and J. M. Liu, Adv. Mater. **23**, 1351 (2011).
[10]C.-H. Yang, J. Seidel, S. Y. Kim, P. B. Rossen, P. Yu, M. Gajek, Y. H. Chu, L. W. Martin, M. B. Holcomb, Q. He, P. Maksymovych, N. Balke, S. V. Kalinin, A. P. Baddorf, S. R. Basu, M. L. Scullin, and R. Ramesh, Nature Mater. **8**, 485 (2009).
[11]J. Wang, J. B. Neaton, H. Zheng, V. Nagarajan, S. B. Ogale, B. Liu, D. Viehland, V. Vaithyanathan, D. G. Schlom, U. V. Waghmare, N. A. Spaldin, K. M. Rabe, M. Wuttig, and R. Ramesh, Science **299**, 1719 (2003).
[12]Y.-H. Lee, J.-M. Wu, Y.-L. Chueh, and L.-J. Chou, Appl. Phys. Lett. **87**, 172901 (2005).
[13]M. Li, F. Zhuge, X. Zhu, K. Yin, J. Wang, Y. Liu, C. He, B. Chen, and R.-W. Li, Nanotechnology **21**, 425202 (2010).
[14]X. Zhu, F. Zhuge, M. Li, K. Yin, Y. Liu, Z. Zuo, B. Chen, and R.-W. Li, J. Phys. D: Appl. Phys. **44**, 415104 (2011).
[15]L. Liu, S. Zhang, Y. Luo, G. Yuan, J. Liu, J. Yin, and Z. Liu, J. Appl. Phys. **111**, 104103 (2012).
[16]X. Chen, G. Wu, H. Zhang, N. Qin, T. Wang, F. Wang, W. Shi, and D. Bao, Appl. Phys. A **100**, 987 (2010).
[17]X. Zou, H. G. Ong, L. You, W. Chen, H. Ding, H. Funakubo, L. Chen, and J. Wang, AIP Adv. **2**, 032166 (2012).
[18]A. Q. Jiang, C. Wang, K. J. Jin, X. B. Liu, J. F. Scott, C. S. Hwang, T. A. Tang, H. B. Lu, and G. Z. Yang, Adv. Mater. **23**, 1277 (2011).
[19]D. Lee, S. H. Baek, T. H. Kim, J.-G. Yoon, C. M. Folkman, C. B. Eom, and T. W. Noh, Phys. Rev. B **84**, 125305 (2011).
[20]C. Wang, K.-J. Jin, Z.-T. Xu, L. Wang, C. Ge, H.-B. Lu, H.-Z. Guo, M. He, and G.-Z. Yang, Appl. Phys. Lett. **98**, 192901 (2011).
[21]A. Tsurumaki, H. Yamada, and A. Sawa, Adv. Funct. Mater. **22**, 1040 (2012).
[22]Z. Hu, Q. Li, M. Li, Q. Wang, Y. Zhu, X. Liu, X. Zhao, Y. Liu, and S. Dong, Appl. Phys. Lett. **102**, 102901 (2013).
[23]S. Hong, T. Choi, J. H. Jeon, Y. Kim, H. Lee, H.-Y. Joo, I. Hwang, J.-S. Kim, S.-O. Kang, S. V. Kalinin, and B. H. Park, Adv. Mater. **25**, 2339 (2013).
[24]S. R. Basu, L. W. Martin, Y. H. Chu, M. Gajek, R. Ramesh, R. C. Rai, X. Xu, and J. L. Musfeldt, Appl. Phys. Lett. **92**, 091905 (2008).
[25]S. J. Clark and J. Robertson, Appl. Phys. Lett. **90**, 132903 (2007).
[26]X. Fang and T. Kobayashi, Appl. Phys. A **69**, S587 (1999).
[27]G.-L. Yuan and J. Wang, Appl. Phys. Lett. **95**, 252904 (2009).
[28]C. Ge, K.-J. Jin, C. Wang, Hui. -B. Lu, C. Wang, and G.-Z. Yang, J. Appl. Phys. **111**, 054104 (2012).
[29]L. Pintilie and M. Alexe, J. Appl. Phys. **98**, 124103 (2005).
[30]L. Pintilie, I. Boerasu, M. J. M. Gomes, T. Zhao, R. Ramesh, and M. Alexe, J. Appl. Phys. **98**, 124104 (2005).
[31]J. F. Scott, in *Ferroelectric Memories*, Advanced Microelectronics Series Vol 103, edited by K. Itoh and T. Sakurai (Springer, Berlin, 2000).
[32]Z.-T. Xu, K.-J. Jin, L. Gu, Y. L. Jin, C. Ge, C. Wang, H. Z. Guo, H.-B. Lu, R.-Q. Zhao, and G.-Z. Yang, Small **8**, 1279 (2012).
[33]S. Asanuma, H. Akoh, H. Yamada, and A. Sawa, Phys. Rev. B **80**, 235113 (2009).
[34]Y. B. Nian, J. Strozier, N. J. Wu, X. Chen, and A. Ignatiev, Phys. Rev. Lett. **98**, 146403 (2007).
[35]O. Bidault, P. Goux, M. Kchikech, M. Belkaoumi, and M. Maglione, Phys. Rev. B **49**, 7868 (1994).
[36]Y. Yang, S. Choi, and W. Lu, Nano Lett. **13**, 2908 (2013).
[37]J. Qi, M. Olmedo, J.-G. Zheng, and J. Liu, Sci. Rep. **3**, 2405 (2013).